Journal of Neural Engineering

Accurate motor mapping in awake common marmosets using micro-electrocorticographical stimulation and stochastic threshold estimation

To cite this article before publication: Akito Kosugi *et al* 2018 *J. Neural Eng.* in press https://doi.org/10.1088/1741-2552/aab307

Accurate motor mapping in awake common marmosets using micro-electrocorticographical stimulation and stochastic threshold estimation

Akito Kosugi[1,3,4], Mitsuaki Takemi[1,3,5], Banty Tia[3,6], Elisa Castagnola[6], Alberto Ansaldo[7], Kenta Sato[1,4], Friedemann Awiszus[8], Kazuhiko Seki[4], Davide Ricci[6], Luciano Fadiga[6,9], Atsushi Iriki[3], Junichi Ushiba[2*]

[1]Graduate School of Science and Technology and [2]Department of Bioscience and Informatics, Faculty of Science and Technology, Keio University, Kanagawa, Japan; [3]Laboratory for Symbolic Cognitive Development, RIKEN Brain Science Institute, Saitama, Japan; [4]Department of Neurophysiology, National Institute of Neuroscience, Tokyo, Japan; [5]Danish Research Centre for Magnetic Resonance, Copenhagen University Hospital Hvidovre, Hvidovre, Denmark; [6]Center for Translational Neurophysiology of Speech and Communication, Istituto Italiano di Tecnologia, Ferrara, Italy; [7]Graphene Labs, Istituto Italiano di Tecnologia, Genoa, Italy; [8]Department of Orthopaedic Surgery, Otto-von-Guericke University, Magdeburg, Germany; [9]Section of Human Physiology, University of Ferrara, Ferrara, Italy.

***Corresponding author:** Junichi Ushiba, Ph.D.

3-14-1 Hiyoshi, Kohoku-ku, Yokohama, Kanagawa, Japan

Tel/Fax: +81-45-566-1678; E-mail: ushiba@brain.bio.keio.ac.jp

Abbreviations[1]

[1] ECR, extensor carpi radialis; ECS, epidural cortical stimulation; EDC, extensor digitorum communis; ICC, intraclass correlation coefficient; ICMS, intracortical microstimulation; IQR, interquartile range; MEPs, motor evoked potentials; ML, maximum likelihood; MSO, maximum stimulator output; μECoG; micro-electrocorticography; MT, motor threshold; PEDOT-CNT, poly-(3,4-ethylene-dioxythiophene) and carbon nanotubes; TB, triceps brachii

Abstract

Objective. Motor map has been widely used as an indicator of motor skills and learning, cortical injury, plasticity, and functional recovery. Cortical stimulation mapping using epidural electrodes is recently adopted for animal studies. However, several technical limitations still remain. Test-retest reliability of epidural cortical stimulation (ECS) mapping has not been examined in detail. Many previous studies defined evoked movements and motor thresholds by visual inspection, and thus, lacked quantitative measurements. A reliable and quantitative motor map is important to elucidate the mechanisms of motor cortical reorganization. The objective of the current study was to perform reliable ECS mapping of motor representations based on the motor thresholds, which were stochastically estimated by motor evoked potentials and chronically implanted micro-electrocorticographical (μECoG) electrode arrays, in common marmosets.

Approach. ECS was applied using the implanted μECoG electrode arrays in three adult common marmosets under awake conditions. Motor evoked potentials were recorded through electromyographical electrodes implanted in upper limb muscles. The motor threshold was calculated through a modified maximum likelihood threshold-hunting algorithm fitted with the recorded data from marmosets. Further, a computer simulation confirmed reliability of the algorithm.

Main results. Computer simulation suggested that the modified maximum likelihood threshold-hunting algorithm enabled to estimate motor threshold with acceptable precision. In vivo ECS mapping showed high test-retest reliability with respect to the excitability and location of the cortical forelimb motor representations.

Significance. Using implanted μECoG electrode arrays and a modified motor threshold-hunting algorithm, we were able to achieve reliable motor mapping in common marmosets with the ECS system.

Keywords: cortical stimulation mapping, ECoG, motor representation, adaptive threshold hunting,

motor threshold, test-retest reliability

1. Introduction

The motor map, i.e., the topographical representation of body movement obtained using intracortical microstimulation (ICMS) over the primary motor cortex, has been widely used as a sensitive indicator of motor skill, learning, and experience, cortical injury and plasticity, and functional recovery (Schieber, 2001; Monfils et al., 2005). The acquisition of motor skill expands the motor map for forelimb movement, which continues to progress as training progresses and reverses once training stops (Nudo et al., 1996; Kleim et al., 1998). The expansion of the motor map has also been demonstrated during the functional recovery from sensorimotor disorders, such as stroke and spinal cord injury (Nudo et al., 1996; Raineteau and Schwab, 2001).

However, motor mapping using ICMS has some intrinsic technical limitations. These include the long experimental procedure, which is at risk of the confounding effect of time, and the inconsistencies in the positioning of the inserted electrode during repeated mapping. Further, the penetrations of the electrode can damage the cortex, causing network dysfunction (Rousche and Normann, 1998; Fernández et al., 2014). Cortical stimulation mapping with epidural electrode arrays has been recently adopted for some animal studies instead of ICMS (Molina-Luna et al., 2007; 2008; Takemi et al., 2017). However, there are also some technical limitations to this approach. The test-retest reliability of epidural cortical stimulation (ECS) mapping has not been examined in detail. The experimental procedure for the long-term evaluation of motor cortical plasticity has not been developed yet. Moreover, many studies have used visual inspection of movement to define the motor threshold (MT), which is an index to compose the motor map; this implies a lack of quantitative measurements. A reliable and quantitative epidural motor map is required to better elucidate the mechanisms of the reorganization of the motor cortex during motor learning or functional recovery after neurological deficit.

The goal of the present study was to perform ECS mapping of motor representation based on the MT, which was stochastically estimated using motor evoked potentials (MEPs). We empirically validated the ECS mapping in adult common marmosets (*Callithrix jacchus*), a small New World monkey. Marmosets have a relatively small body size, are easy to handle, and are characterized by fast sexual maturation, with the added advantage of providing unique behavioral and cognitive characteristics (Okano et al., 2012) that satisfy the requirement for preclinical animal studies. Several experimental techniques employed in rodents, such as motor function test (Takemi et al., 2014), calcium imaging (Sadakane et al., 2015), and optogenetics (MacDougall et al., 2016), can be used, either directly or after a slight modification, in these small-bodied primates. The nearly lissencephalic cortex allows easy access to the sensorimotor cortex for the electrophysiological assessment using an array of surface electrodes (Huffman and Krubitzer, 2001). Unlike rodents, however, marmosets have a well-developed frontal cortex and, like humans, show clear separation of the primary motor cortex from the somatosensory cortex (Burman et al., 2008). In the present study, micro-electrocorticographical (μECoG) electrode arrays were chronically implanted over the sensorimotor cortex, while electromyographical (EMG) electrodes were inserted into upper limb muscles to detect twitches. The stochastic threshold estimation algorithm was validated in vivo electrophysiology experiments fitted with the recorded data from marmosets. Further, reliability of the algorithm was additionally confirmed by an in silico computer simulation. The current study enabled us to understand the basic properties of functional motor representations in the common marmoset, which could then be extended to phylogenetically higher species as well.

2. Material and Methods

2.1. Animals

Three adult male common marmosets (*Callithrix jacchus*; MK1, 358 g; MK2, 356 g; MK3, 380 g) were used in the present study. MK1 and MK2 were shared with a study that tested grasping-related

cortical activities (Tia et al., 2017) but the grasping experiments were conducted after data acquisition for this study was accomplished. All procedures were performed in accordance with the Laboratory Animal Welfare Act and The Guide for the Care and Use of Laboratory Animals (National Institutes of Health, Bethesda, MD) and were approved by the Institutional Animal Research Committee at RIKEN (IRB approval number H24-2-228).

2.2. Electrode array

We implanted μECoG electrode arrays that were coated with a nanocomposite of poly-(3,4-ethylene-dioxythiophene) and carbon nanotubes (PEDOT-CNT) and encapsulated by fibrin hydrogel (Castagnola et al., 2013; 2014). The use of nanomaterial coatings reduced electrode impedance and increased charge injection capacity. μECoG electrode arrays used in the current study were custom-made (6.8 × 8.0 mm; Fig. 1A). The size was defined enough to cover the upper limb area of the sensorimotor cortex in marmosets (Burish et al., 2008; Burman et al., 2008; Kondo et al., 2015). The arrays had 64 channel electrodes, each of which had a diameter of 0.1 mm. The distance between each electrode was 0.9 mm and 0.7 mm, in the mediolateral and anteroposterior directions, respectively. They also had four stimulation ground contacts (diameter, 0.5 mm).

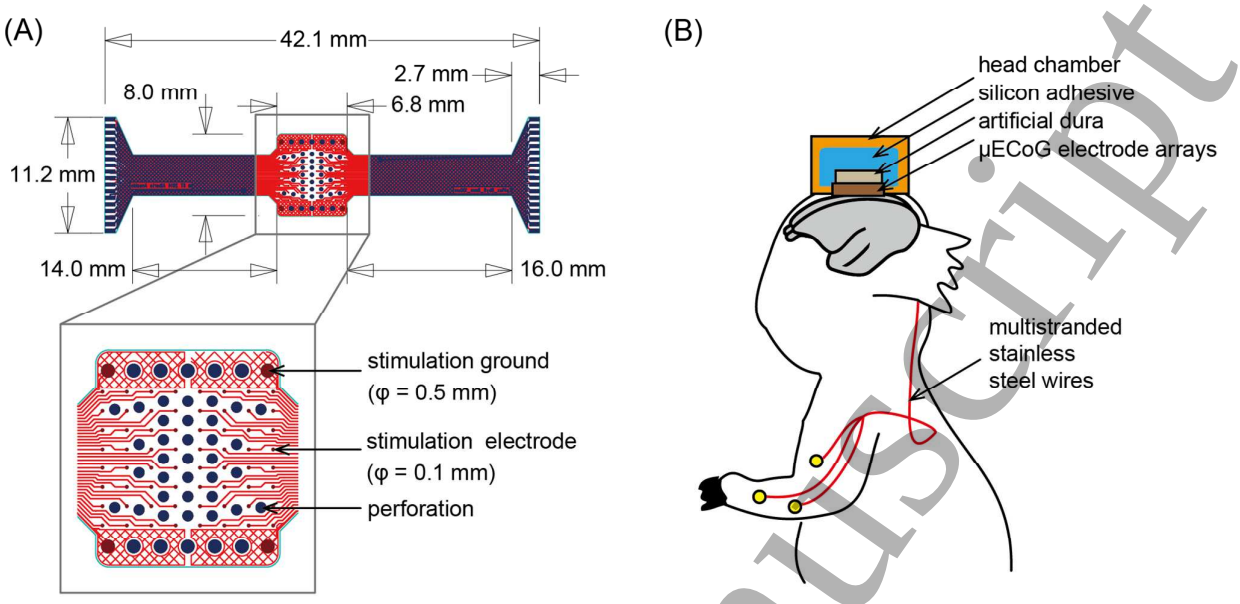

Figure 1. (A) Micro-electrocorticographical (μECoG) electrode arrays were coated with a nanocomposite of poly-(3,4-ethylene-dioxythiophene) and carbon nanotubes (PEDOT-CNT) and encapsulated by fibrin hydrogel. The arrays had 64 channel electrodes and 4 stimulation grounds. (B) Schematic drawing of implantation of electromyographical electrodes and μECoG electrode arrays. Red lines represent multi-stranded stainless steel wires implanted subcutaneously in the target muscles. The arrays were placed in the chamber and the inside of the chamber was filled with silicone polymer.

2.3. Surgical procedure of μECoG and EMG electrode implantation

Implantation of μECoG electrode arrays and EMG wire electrodes were performed on different days under anesthesia. Anesthesia was induced by an intraperitoneal injection of medetomidine/midazolam/butorphanol (0.05, 0.5, and 0.5 mg/kg, respectively). Atropine (0.10 mg/kg) and prednisolone (0.15 mg/kg) were intramuscularly injected immediately after the anesthesia. During the surgery, anesthesia was maintained by inhalation of 1.5–2.5% isoflurane and the oxygen saturation level was continuously monitored.

For implantation of μECoG electrode arrays, a craniotomy of 9 × 5 mm (coordinates relative to Bregma as follows: 0–9 mm anterior and 2–7 mm lateral) was performed in the left hemisphere, ensuring that the dura mater was maintained intact. The μECoG electrode arrays were implanted between the dura and skull. The arrays were laid onto the dura using a micromanipulator. A piece of artificial dura mater was then applied between the arrays and the skull. The head chamber was made of Ultem, which is a polyetherimide polymer characterized by high dielectric, solvent resistance, and mechanical properties. The chamber was attached to the skull with stainless steel screws and dental acrylic, to hold the electrode connectors. The inside of the chamber was filled with silicone polymer (Kwik-Cast, World Precision Instruments, Sarasota, FL; Fig. 1B).

The protocol to implant EMG wire electrodes was based on previous studies (Park et al., 2000; Hudson et al., 2010). Briefly, pairs of multi-stranded stainless steel wires (AS634, Cooner Wire, Chatsworth, CA) were implanted subcutaneously in the following target muscles of the right upper limb: deltoid, triceps brachii (TB), biceps brachii (only one marmoset), extensor carpi radialis (ECR), flexor carpi radialis (only one marmoset), extensor digitorum communis (EDC), and flexor digitorum superficialis. The location of each muscle was identified by its anatomical features and the movements elicited by trains of low-intensity electrical stimulation. Two electrodes, spaced 5 mm apart, were implanted in each muscle.

2.4. Cortical stimulation

Stimulus current was generated by the isolator output (SS-203J; Nihon Kohden, Tokyo, Japan) and controlled from the analog output module (NI PCIe-6321; National Instruments, Austin, TX). In the present study, the stimulus was composed of five 250-μs biphasic cathodal and anodal pulses delivered at 1,000 Hz with a maximum stimulator output (MSO) of 1.0 mA. The pulse repetition rate at 1,000 Hz (1 ms interpulse interval) is much higher than the period of re-polarization after neuronal discharge. However, it was considered that increasing the stimulation frequency for increasing the number of pulses might efficiently activate pyramidal cells even though the pulse repetition was more than the rate of re-polarization.

The EMG signals were band-pass filtered (1–2,000 Hz with 2nd order Butterworth) and digitized at 4,800 Hz using an amplifier (g.USBamp; g.tec medical engineering GmbH, Graz, Austria). During cortical stimulation, marmosets held onto the pole and were kept awake and resting. The animals were wearing jacket and the jacket was fixed with the pole and the limbs also touched the pole. We set the permissible background EMG amplitude to continue cortical stimulation mapping to be at 50 μV. If the peak-to-peak amplitude of deltoid, TB, ECR, or EDC muscles exceeded 50 μV within last 80 ms, it was deemed that voluntary muscle activity had occurred and the stimulation was automatically stopped until termination of voluntary muscle activity. MEP amplitudes were calculated online and the next stimulation intensity was then selected using an in-house developed algorithm (see next section), which was written with MATLAB 2013a (MathWorks, Natick, MA). The stimulation channel was also selected randomly out of 64 channels at every trial. These processes were repeated until the MT of all μECoG channels was determined.

2.5. Motor threshold estimation

2.5.1. Algorithm for motor threshold estimation

The MT was generally defined as a stimulus intensity at which a significant MEP can be obtained

with a probability of 50% (Rossini et al., 1994). In the current study, we determined the MT using the Maximum Likelihood (ML) threshold-hunting approach (Awiszus, 2003), which is summarized below. The MT was estimated based on fitting the cumulative Gaussian distribution on the measured probability of MEPs with different stimulation intensities.

The probability, p, to obtain a significant MEP at a particular stimulus intensity, m, was modeled by a cumulative Gaussian as follows:

$$p(m,t,s)=\frac{1}{s\sqrt{2\pi}}\int_{-\infty}^{m} e^{\frac{(\tau-t)^2}{2s^2}}d\tau$$

where t is the "threshold" corresponding to the stimulus intensity at which p = 0.5, and s is the "threshold spread" corresponding to the extra amount of stimulus intensity required to increase the p from 0.5 to 0.84. The log-likelihood function, L, after n stimuli were applied was calculated as follows:

$$L(t,s)=\sum_{i=1}^{j}\ln(1-p(ms_i,t,s))+\sum_{i=1}^{k}\ln(p(mf_i,t,s))$$

where *ms* and *mf* were the stimulus intensities that succeeded or fail to obtain MEP, respectively, and j and k were the numbers of stimuli corresponding to *ms* and *mf*, respectively (where $j + k = n$). The values of t and s that maximized L were identified. The stimulation intensity for the subsequent stimulus was then automatically set that maximized $L(m, 0.07m)$. The threshold spread parameter, which was here defined as 7% of the underlying threshold, was also tested in our experimental condition using pre-measured MEP data. ECS was applied to two different μECoG channels at 10 different stimulus intensities. At each intensity, 10 MEPs were recorded from the deltoid and EDC muscles. The probabilities to obtain significant MEPs were calculated and fitted to a cumulative Gaussian distribution (Fig. 2C).

2.5.2. Modification of the threshold estimation procedures and its test of feasibility by Monte-Carlo simulation

Since the ML regression algorithm estimates the refined MT, with a smaller number of stimuli (Mishory et al., 2004), it results in less robust estimate under considerable background EMG activity (Qi et al., 2011). Modification of the ML threshold-hunting algorithm makes it useful for animal experiments, because awake animals are difficult to maintain at rest, especially after strong stimulations that induce large body movement. Thus, we modified the algorithm using the three following directions: (1) changing the setting rule of the next stimulus intensity, (2) reducing the number of prior samples of MEP results for threshold estimation, and (3) changing the stopping criterion for threshold estimation. Thus, the modified ML threshold-hunting algorithm had five steps as outlined below.

STEP 1: Two "pseudo responses" (no MEP at 15% and significant MEP at 105% of MSO) was set to identify the interval within which the threshold hunting procedure was conducted and to determine the initial stimulus intensity. The initial stimulus intensity, m_1, which maximized L was identified (m_1, $0.07m_1$). This was set to 35% of MSO.

STEP 2: A stimulus was applied. Peak-to-peak MEP amplitude of a target muscle in a period of 10–20 ms after the stimulus was calculated to determine whether it exceeded the predetermined threshold (60 μV). We set the threshold of MEP at 1.2 times higher than the permissible background EMG amplitude in order to minimize false positive MEP detection.

STEP 3: The estimated MT was calculated. $L(t, 0.07t)$ was maximized with the given number of prior samples of MEP results.

STEP 4: The next stimulus intensity, m_{n+1}, was calculated as follows. The ideal next stimulus intensity, M, which maximized $L(M, 0.07M)$ was first calculated. Next, if the M was larger than the previous stimulus, m_n, by 10% of MSO, then m_{n+1} was set to m_n+10% MSO. If the MEP did not exceed the predetermined threshold for the last four stimuli, then m_{n+1} was also set to m_n+10% MSO. Finally, if all the above conditions were false, then m_{n+1} was set to M.

STEP 5: STEPS 2, 3, and 4 were executed until a given number of stimuli was applied. The

stimulation was then stopped and the MT that maximized $L(t, 0.07t)$ was determined.

The number of prior samples used for threshold estimation and the number of stimuli required to stop the threshold estimation procedure were determined using a Monte-Carlo simulation. First, two uniform random numbers, r_1 and r_2, were generated in the interval (0, 1). The quantity r_1 stood for the simulated MEP. If $p(m, t, s)$ was smaller than r_1, the simulated response was classified as a success; if it was larger or equal to r_1, it was classified as a failure. The quantity t was set within the ordinary experimental ranges (from 25–95% MSO). The quantity, r_2, stood for the simulated muscle activity that was not induced by stimulation. If r_2 was smaller than a given number, r, (here defined as 0.1), the simulated MEP was classified as "pseudo" MEP, irrespective of the r_1 value. The probability of pseudo-MEP occurrence was determined using EMG data measured from the four upper limb muscles (i.e., deltoid, TB, ECR, and EDC). The data consisted of 50 trials of EMG data time-locked to the stimulation, which was applied for each of the 21 μECoG electrodes, where the MEP was never induced by the stimulation at 100% MSO. We visually determined the pseudo MEP and calculated the probability of pseudo-MEP occurrence for each electrode and each muscle. The 95th percentile of the probability was extracted from 84 samples (21 μECoG channel × four upper limb muscles) for defining the given number, r (Fig. 2A and B).

A total of 50 simulated responses were generated to evaluate the following two types of threshold-estimation procedures: (1) modified ML threshold-hunting algorithm, which uses 8 to 18 responses prior to the current response, and (2) the conventional ML hunting, which takes all previous responses into account. Each of the threshold estimation procedures was repeated 10,000 times. For each estimated threshold value, t_e, the error value e was calculated as $e = |t - t_e|$. The 95% error limit obtained as the 95th percentile of the 10,000 error values was evaluated for each threshold estimation procedure.

2.6. Test-retest reliability of motor map measurements

The reliability of the maps was assessed using intraclass correlation coefficients (ICCs). The ICC assesses the within-day or between-day variability (values range from 0 to 1), where values ≥ 0.80 are considered reliable (Landis and Koch, 1977; Shrout and Fleiss, 1979; McGraw and Wong, 1996). We calculated the ICC of four different types of motor map indices, which have been used in human transcranial magnetic stimulation studies in order to evaluate cortical excitability, location of the hotspot (i.e., the electrode position where the lowest MT was observed), and the relationship of the cortical forelimb motor representations between each muscle as follows: (1) minimum MT, (2) map area, (3) normalized map volume, and (4) overlapping area (Wolf et al., 2004; Ngomo et al., 2012; van de Ruit et al., 2015). The map area was calculated as the number of electrodes in which the MT was lower than a certain value, which ranged between 65% and 95% MSO with 10% MSO steps. The normalized map volume was calculated by the sum of MTs ($\leq$ 65% MSO), normalized to the minimum MT. The overlapping area was the number of the active electrodes (MT $\leq$ 65% MSO) in both the deltoid and EDC muscles. We chose a 65% MSO as the maximum MT used for calculation of the normalized map volume and the overlapping area, since the ICC(1,1) and ICC(2,1), which reflected intra-day reliability and between-days reliability, respectively, always exceeded 0.80 if the electrodes with MTs below 65% MSO were used for the calculation.

3. Results

3.1. Threshold property

Figure 2A shows typical examples of a significant MEP and a pseudo MEP. The significant MEP exceeded the predetermined amplitude within a certain period of time after stimulation. A pseudo MEP generally showed spiky muscle activity that was not induced by stimulation and was indistinguishable from a significant MEP in terms of its shape and amplitude. Even if the stimulation stopped while voluntary muscle activity was being observed, the spiky muscle activity still occurred.

Therefore, the spiky muscle activity caused a false positive increase of the probability of MEP occurrence. The 95th percentile of probabilities of pseudo-MEP occurrences was 10% (Fig. 2B). According to this result, the probability of pseudo MEP in the Monte-Carlo simulations was set to 0.1.

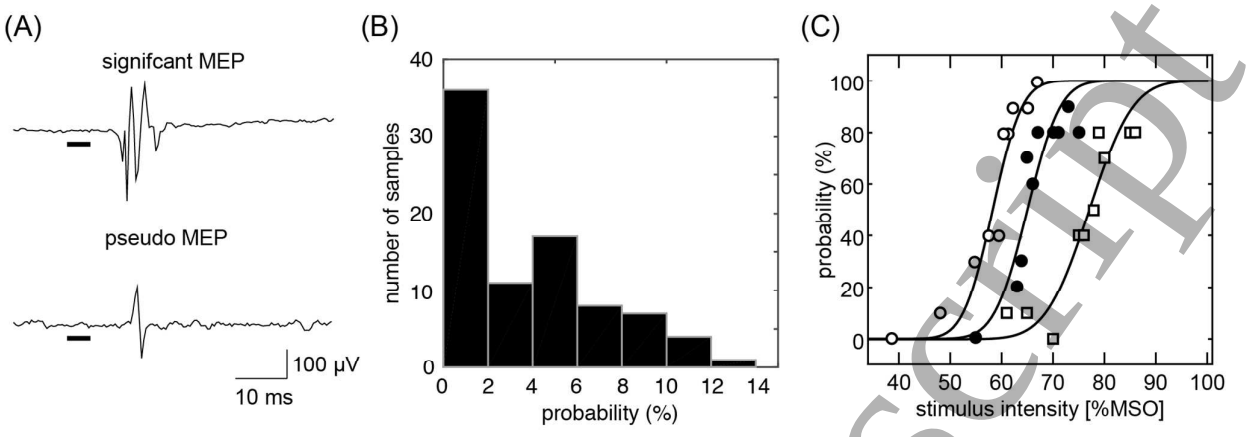

Figure 2. (A) Typical examples of a significant motor evoked potential (MEP) and pseudo MEP. The significant MEP exceeded the predetermined amplitude (60 μV) after stimulation. The pseudo MEP generally showed spiky muscle activity, which was not induced by stimulation. Black bars below MEP waveforms represented a period of stimulation. (B) Histogram of the probabilities of pseudo MEP occurrence. (C) Cumulative Gaussian distribution of the probability in obtaining significant MEPs. The results of the curve fittings are shown with open circles, filled circles, and open squares. Circle symbols represented values derived from the extensor digitorum communis (EDC) responses. Open circles and filled circles indicated results from different stimulation channels. Square symbols represented values derived from the deltoid muscle response.

The measured probabilities to obtain significant MEPs were well fitted to a cumulative Gaussian distribution (Fig. 2C). Circle symbols represented values obtained from the EDC. Thresholds were 55.7% and 65.0% MSO, while threshold spreads were 4.8% and 5.0% MSO. Square symbols represented values obtained from the deltoid. The threshold was 77.1% and the threshold spread was 6.7% MSO. The relative threshold spreads of these data were 8.6%, 7.8%, and 8.7% MSO. We then confirmed that the motor thresholds derived using 7% and 8% MSO as relative threshold spread were almost identical (Supplementary Fig. 1). Thus, we intended to develop the threshold-hunting algorithm for marmosets using a relative threshold spread of 7%, which was consistent with humans (Awiszus, 2003), enabling broad application.

3.2. In silico: Monte-Carlo simulations

Monte-Carlo simulations were performed to determine the number of samples and number of stimuli required for accurately estimating the MT. The results of simulation at three different thresholds are shown in Fig. 3. When all prior samples were used for threshold estimation, the error limits became larger, especially when the true threshold was high. In the simulation with the true threshold at 45% MSO (Fig. 3A), the error limits fell below ±6.5% MSO with many numbers of prior samples when more than 19 stimuli were applied. The simulations of true thresholds at 65% and 85% MSO showed error limits remaining high and did not fall below ±6.5% MSO when the number of prior samples was less than 12 (Fig. 3B and C). Therefore, we set the optimal number of samples for threshold estimation to 12 and the optimal number of stimuli to 20. Figure 4A shows the stopping error by using these parameters. The results demonstrated that although the MT tended to be underestimated, the interquartile range (IQR) of the stopping errors was less than ±5% MSO. Moreover, the lowest estimated threshold within 1.5×IQR of the lower quartile was smaller than 6.5% MSO below the true threshold, when the true threshold was 25–65% MSO.

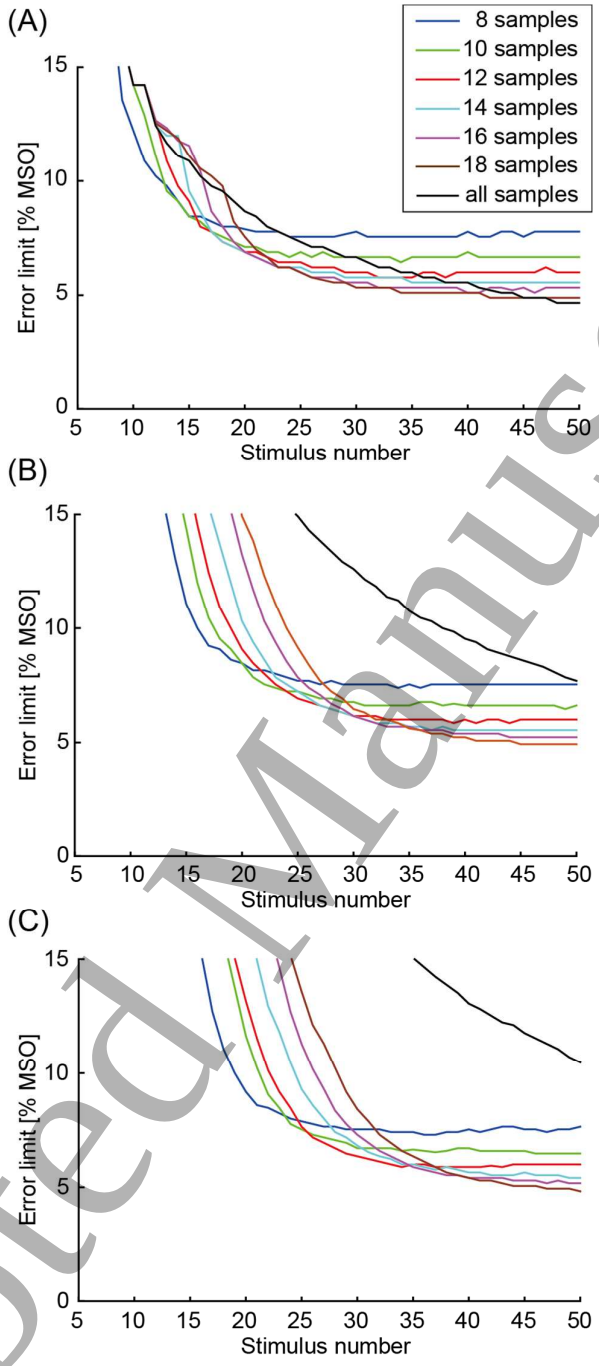

Figure 3. Relationship between the estimated error limits and stimulus number. Monte-Carlo simulations were performed on true thresholds set to (A) 45%, (B) 65%, and (C) 85% of maximum stimulator output (MSO). Each colored line represents the result of using different numbers of prior samples in the threshold hunting procedure.

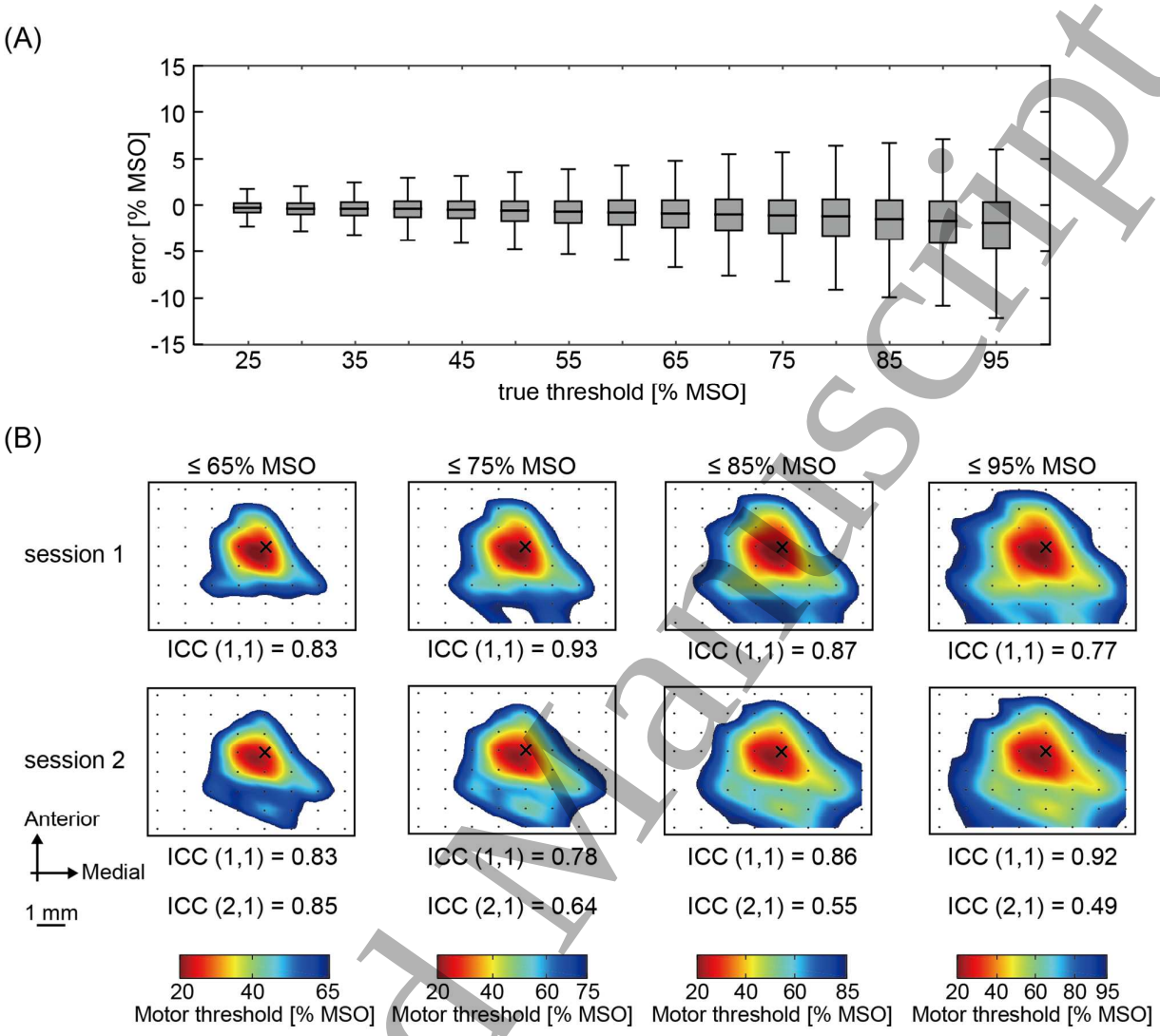

Figure 4. Assessment of the reliability of the modified maximum likelihood (ML) threshold hunting algorithm (A) in silico and (B) in vivo. (A) Stopping error in the modified ML threshold-hunting algorithm estimated by the Monte-Carlo simulation that repeated 10,000 times. The number of samples used for threshold estimation was set to 12 and the number of stimuli was set to 20. Box plots indicate the median (black line in the box), interquartile range (IQR; gray box) and the lowest and highest data within 1.5 IQR of the lower and upper quartile, respectively (error bars). (B) Stability of the motor map over time. The maps of deltoid muscle of a single marmoset (MK1) are shown. The geometry of the motor map remained stable across two sessions. Intraclass correlation coefficient (ICC) of the map area was calculated as a number of electrodes of which the motor

thresholds were less than a certain value (65–95% of MSO with a step-size of 10% MSO). ICC(1,1) and ICC(2,1) reflect the test-retest reliability within and between sessions, respectively. Black dots indicate the position of the stimulus electrodes. Black crosses indicate the hotspot (an electrode position where the lowest motor threshold was observed).

3.3. In vivo: motor mappings

Implantation of μECoG and EMG electrodes, cortical stimulation, and motor mapping were successfully performed in all three marmosets. MTs were also successfully determined for all channels and for all muscles, but here we only showed the motor maps of the deltoid and EDC, which are the most proximal and the most distal muscles in the present study, respectively, to avoid confusion. Both within- and between-session test-retest reliability of the motor maps were assessed. A single session consisted of four ECS mappings performed within one day, with two repeated sessions after an interval of 3-4 days. The first session was performed at least 2 weeks after the μECoG array implantation.

The ICC of the map area was calculated using the electrodes, in which the MTs were less than 65%, 75%, 85%, and 95% MSO. We found that both good within- and between-session reliability (ICC $\geq$ 0.80) were observed if the electrodes with a MT that was less than 65% MSO were used for the map area calculation (Fig. 4B). These results were consistent across different forelimb muscles, so we decided to use electrodes with a MT less than 65% MSO for further comparison and evaluation of ICC across types of the motor map indices.

The ICC(1,1), which reflected the within-session test-retest reliability, indicated that the map area and normalized map volume were reliable for both deltoid and EDC muscles. The minimum MT of the EDC muscle was also reliable, but that of the deltoid muscle slightly varied within sessions. The overlapping area was not reliable within session 1 and 2. Between the two sessions, all the motor map indices were reliable, which suggested that the hotspot and geometry of motor maps were stable between days (Fig. 4B). These results are summarized in Table 1. Figure 5 shows the average forelimb motor maps in a single marmoset (MK1). We obtained the different topographic profiles of the MTs over the channels for the two forelimb muscles simultaneously. These maps were partially overlapped (overlapping area: 58±11%). The hotspot was different between deltoid and EDC muscles. Although not quantitatively demonstrated, there appeared to be a

trend in the relative positions of deltoid and EDC, with the hotspot of deltoid motor map located anterior to that of the EDC motor map. The motor maps in the other marmosets are shown in Supplementary Fig. 2.

Table 1

Reliability of the motor map measurements within and between sessions.

	Mean ± SD		ICC(1,1): within-session		ICC(2,1): between-session
	Session 1	Session 2	Session 1	Session 2	
Minimum MT (deltoid) [% MSO]	36±10	39±10	0.80	0.79	0.89
Minimum MT (EDC) [% MSO]	39±14	39±13	0.93	0.88	0.99
Map area (deltoid)	13±4	11±8	0.83	0.83	0.85
Map area (EDC)	13±9	11±10	0.96	0.96	0.98
Normalized map volume (deltoid)	27.8±13.4	21.3±18.4	0.91	0.87	0.89
Normalized map volume (EDC)	29.0±31.3	25.1±30.0	0.97	0.96	0.99
Overlapping area (%)	37±22	47±16	0.76	0.51	0.86

EDC, extensor digitorum communis; ICC, intraclass correlation coefficient; MSO, maximum stimulator output; MT, motor threshold; SD, standard deviation

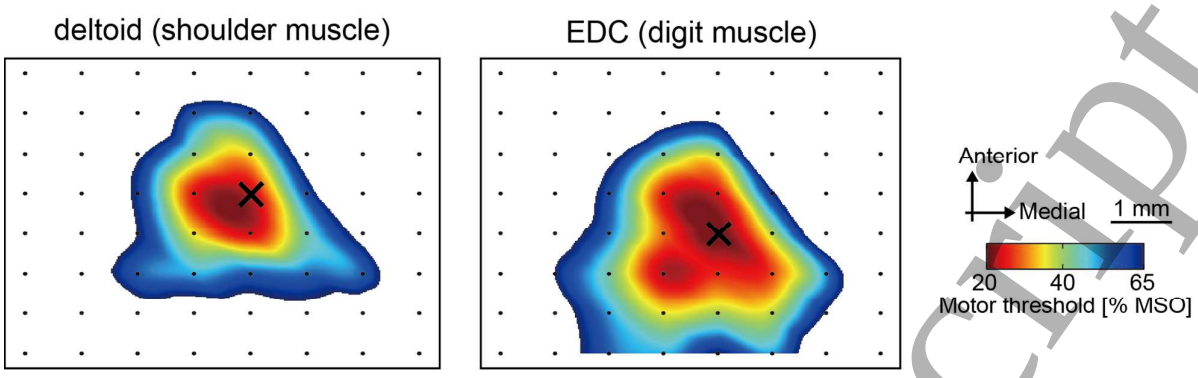

Figure 5. Averaged motor maps of the two forelimb muscles. Estimated motor thresholds were used as the index of motor representation and spatially interpolated. Black dots indicate the position of the stimulus electrodes. Black crosses indicate the hotspot.

4. Discussion

In the current work we succeeded in developing a novel method for mapping motor representations in common marmosets, based on a MT that was stochastically estimated using the ML method. Implantation of the EMG electrodes and μECoG electrode arrays allowed repeated mapping of the same cortical areas. Modification of the ML threshold-hunting algorithm enabled us to estimate MTs, with acceptable precision both in silico and in vivo. ECS mapping showed high reliability with respect to the between-day cortical excitability and both within- and between-day location of the cortical forelimb motor representation.

4.1. Feasibility of the modified threshold-estimation procedures

Several computer simulation studies showed that ML hunting algorithm estimated the MT faster and more precisely than other conventional threshold-determining methods. Recently, ML hunting has also been widely used in human preclinical studies (Awiszus, 2003; Borckardt et al., 2006; Qi et al., 2011). In the present study, we revisited the original ML algorithm, since animals cannot stay at rest for a long time, which increases false positive detection. Our simulation results demonstrated that the modified threshold estimation algorithm allowed an acceptable MT to be determined in animal models. However, it should be also noted that our algorithm cannot reach the same level of accuracy as the original ML threshold-hunting approach (Awiszus, 2011), unless a pseudo MEP is distinguished from a stimulus-induced MEP automatically.

The original ML regression algorithm was designed with the assumption that all inputs were reliable (Pentland, 1980), which is hardly the case for animal experiments. In order to counteract false observations, such as pseudo MEP, our method restricted the number of prior MEPs used for updating the next stimulus intensity and the step size used to shift the intensity. According to the simulation results, 12 prior MEPs were suggested as allowing an appropriate balance between the number of stimuli and accurate threshold estimation. In-vivo mapping experiments further provided

evidence that a MT lower than 65% MSO was reliable when 20 stimuli were applied. One may try to estimate MT with less than 20 stimuli due to difficulties, such as an animal has not been well trained to maintain at rest, but this will increase a difference between the true threshold and estimated threshold (Fig. 3). The trade-off between the estimation accuracy and the number of stimuli must be taken with caution. Considering the stochastic nature of the ML algorithm, a case with a lower true threshold was less affected by pseudo MEPs. Mathematically, an MEP with a stimulus intensity that is lower than the true threshold is highly likely to be a false positive, since a significant MEP is less likely to be provoked. This means that a higher true threshold was higher is more likely to result in a pseudo MEP, resulting in a less accurate estimation.

In the ML hunting procedure with the initial setting of no MEP at 15% and significant MEP at 105% MSO, the first stimulus intensity was fixed at 35% MSO. If an MEP was not obtained with the first stimulus, the second intensity was set to 45% due to the step size restriction to shift the intensity. If an MEP was also not obtained with the second stimulus, the third intensity was set to 55%. Again, these initial results are likely to be false positives, since an MEP with a relatively low intensity compared to a true threshold is more likely to be a pseudo MEP. Restricting the number of prior MEPs avoids usage of these false positive data, which subsequently ensures that the estimated threshold is close to the true value. Furthermore, without this restriction, if pseudo MEPs occur during initial stimulation, it is challenging to reach high stimulus intensity in subsequent estimations when using the original ML algorithm.

4.2. Map reliability

Our results showed high test-retest reliability of motor map measurements. For example, the ICC of the map area and normalized map volume, which reflect size consistency of the cortical motor map, showed excellent reliability both within- and between-days regardless of the muscle that was analyzed. In addition, the minimum MT, an index of the cortical excitability, was stable between sessions in both the deltoid and EDC muscles. These results corroborated with previous transcranial

magnetic stimulation studies that reported good reliability of MT in humans (Carroll et al., 2001; Malcolm et al., 2006; Ngomo et al., 2012) and animals (Amaya et al., 2010). Our results also suggested that the within-session reliability of the minimum MT was more variable for the proximal muscle compared to the distal muscle. We presumed that this was caused by differences in the trial-to-trial MEP variability, as proximal muscles showed more variable MEP responses, in comparison with distal muscles (Brasil-Neto et al., 1992). It must be noted that the location of forelimb cortical representation identified by our method was consistent with previous cytoarchitectural and electrophysiological studies investigating the motor areas in the marmoset cortex (Burish et al., 2008; Burman et al., 2008).

The map area did not show good reliability when it was calculated using the electrodes in which the MT was above 65% MSO. Thus, the estimated threshold was less consistent with higher stimulus intensities. This is in line with the result of our Monte-Carlo simulation indicating that a larger threshold resulted in greater error limits. In particular, the lowest error of the estimated threshold within 1.5×IQR of the lower quartile became smaller than 5% MSO below true threshold, if the true thresholds were higher than 65% MSO. Considering that MEP variability increases as the stimulation site becomes more distant from the hotspot (Brasil-Neto et al., 1992), muscle responses to cortical stimulation at the sites in which the estimated MTs exceeded 65% MSO might be unstable. This could be another cause for lower test-retest reliability of the map area calculated using the electrodes with the MTs above 65% MSO.

The results described here were assessed across two sessions separated by 3–4 days. Yet, long-term reliability of ECS mapping is still unclear. Effect of time on the growth of dura in response to the array implantation in marmosets needs to be studied for long-term stimulation mapping procedure. A previous study reported that electrode impedance increased due to the tissue reaction from few days and up to a maximum of 1 week after the initial implantation of Michigan silicon microelectrodes covered with PEDOT films (Ludwig et al. 2006). We started the stimulation mapping experiments more than 1 week after the implantation surgery, so impedance changes due to

tissue reaction should have already stabilized.

4.3. Advantages and limitation of epidural cortical stimulation mapping

One advantage of our mapping system is that it is capable of characterizing the motor cortex in awake animals. Since anesthesia induces significant changes of amplitude and latency of MEPs (Chiba et al., 1998; Zandieh et al., 2003), it is desirable to avoid animals being anesthetized. Our mapping system reduced the duration required to create motor maps to less than 10 min. This may be a reason why our mapping was successful in awake animals who are difficult to keep at rest for a longer period of time.

The other advantage of this approach was the low invasiveness. According to a previous histological study performed after ECS, no cortical damage or motor deficits were observed in the animals even after repeated stimulations (Molina-Luna et al., 2007). In the current study, no motor deficits were observed in any of the animals as well. In addition, our results suggest that electrode positioning between repeated mapping sessions remained consistent. These are fundamental prerequisites for the longitudinal evaluation of motor cortical plasticity after motor learning or functional recovery after sensorimotor disorders.

One technical limitation of stimulating epidurally is the current spread. The resolution of epidural current spread in marmosets is not known. However, the dura of marmosets is thin compared to humans and macaque monkeys (Bourne and Rosa, 2003; Lui et al., 2014) and similar to those in rats, where the resolution of epidural and subdural current spread is almost identical (Slutzky et al., 2010). We therefore presumed that motor mapping with epidural stimulation in marmosets could be almost identical to the subdural stimulation. Because of the same reason, a distance between electrodes was designed in concordance with a previous study investigating the optimal spacing for epidural stimulation and recording in rats (Slutzky et al., 2010).

Another limitation of stimulating epidurally is the need for higher stimulation currents to

surpass the MT of cortical neurons, than those required by ICMS. ECS may activate cortical interneurons and trans-synaptically activate pyramidal neurons since axons are more excitable than cell bodies or dendrites (Wongsarnpigoon and Grill, 2012). Although we previously demonstrated that the maps identified by ICMS and ECS were statistically correlated (Takemi et al., 2017), it should take into account a difference in the mechanism activating neurons between ICMS, mostly direct stimulation to cell bodies, and cortical surface stimulation. Higher current stimulation may also cause the involuntary muscle contraction from a reaction to noxious stimulation of dura. However, considering a time for signal transmission in the sensory-motor loop, it is hardly considered that the MEP occurring within 10−20 ms following ECS stems from noxious stimulation or painful sensation. An EMG implantation to the ipsilateral limb will further help to ensure that MEP provoked by ECS is mediated by motor pathways.

4.4 *Future work*

One may consider using the current algorithm for simultaneous estimation of corticomotor representations of multiple muscles. In this study, we developed the algorithm to estimate one motor map in a single mapping session, but we should be aware of that MEP amplitudes had been always recorded from all four muscles. It is possible to roughly estimate MTs of non-target muscles by fitting the MEP amplitudes collected during a mapping of target muscle to the modified ML algorithm. However, since the stimulus intensity is not optimized for the estimation of MTs of non-target muscles, it requires additional stimulations to reach the error limits below ±6.5% MSO. There is trade-off relationship between a time required for mapping and number of motor representations estimating, although the duration would not simply increase as a function of the number of estimated representations.

It is also required to improve false positive MEP detection. The current algorithm was designed as if the pseudo MEP is observed in 10% of total stimulations. The pseudo MEP refers to

spiky EMG activity not induced by cortical stimulation, which occurs in a time window for calculating MEP amplitude. Therefore, the pseudo MEP is a false positive and significantly hampers accuracy of the MT estimation. Supervised learning with sufficient amount of labeled training data could pave the way for better discrimination between the pseudo and the true significant MEP, which is provoked by cortical stimulation activating motor pathways. This will result in reduction of the false-positive ratio and may enable more reliable mapping by less than 20 stimuli per point and to predict MT of more than 65% MSO.

5. Conclusion

In the current study, we established reliable epicortical stimulation mapping for the motor somatotopy and proved it in three common marmosets after chronic implantation of EMG and μECoG electrodes. The results of both in silico computer simulation and in vivo electrophysiology experiments demonstrated that MT could be stochastically estimated by means of the modified ML method with acceptable precision. We modified a setting rule of the next stimulus intensity to avoid excessive contractions of muscles and restricted a number of prior MEPs used for MT estimation. This approach represented a reasonable compromise between robustness and accuracy, making our ML modifications a standard of MT estimation procedure for animal experiments in the future. In addition, in vivo ECS mapping performed with the marmosets showed that the MT was estimated constant between days and the location of the forelimb corticomotor representation was stable both within a day and between days. These findings suggested that our ECS system allowed repeated mapping of a given cortical area, which will enable us to elucidate the mechanism of day-by-day reorganization of the motor cortex, during motor learning or functional recovery from neurological deficits.

Acknowledgments

We thank Dr. Takahiro Kondo and Dr. Kimika Yoshino for advice on the surgical procedure and Dr. Yumiko Yamazaki, Mr. Masakado Saiki, Mr. Masayuki Inada, Mr. Taku Koike and Mr. Takafumi Nakamura for their technical assistance.

Conflict of interest

Atsushi Iriki is the President and CEO of Rikaenalysis Corporation (RIKEN Venture). The other authors declared no competing financial interests.

Funding

This work was supported by Grants-in-Aid for JSPS Research Fellow to A.K. (#15J05875) and M.T. (#14J00630), the Brain/MINDS project from AMED, Japan to A.I. and grants from the Italian Ministry of the University and Research to L.F.

References

Amaya F, Paulus W, Treue S and Liebetanz D 2010 Transcranial magnetic stimulation and PAS-induced cortical neuroplasticity in the awake rhesus monkey *Clin. Neurophysiol.* 121 2143-51

Awiszus F 2003 TMS and threshold hunting *Suppl. Clin. Neurophysiol.* 56 13-23

Awiszus F 2011 Fast estimation of transcranial magnetic stimulation motor threshold: is it safe? *Brain Stimul.* 4 58–9

Borckardt JJ, Nahas Z, Koola J and George MS 2006 Estimating resting motor thresholds in transcranial magnetic stimulation research and practice. A computer simulation evaluation of best methods *J. ECT* 22 169–75

Bourne JA and Rosa MG 2003 Preparation for the in vivo recording of neuronal responses in the visual cortex of anaesthetised marmosets (*Callithrix jacchus*) *Brain Res. Protoc*. 11 168-77

Brasil-Neto JP, McShane LM, Fuhr P, Hallet M, and Cohen L 1992 Topographic mapping of the human motor cortex with magnetic stimulation: factors affecting accuracy and reproducibility *Electroencephalogr. Clin. Neurophysiol.* 85 9–16

Burish MJ, Stepniewska I and Kaas JH 2008 Microstimulation and architectonics of frontoparietal cortex in common marmosets (Callithrix jacchus) *J. Comp. Neurol.* 507 1151-68

Burman KJ, Palmer SM, Gamberini M, Spitzer MW and Rosa MG 2008 Anatomical and physiological definition of the motor cortex of the marmoset monkey *J. Comp. Neurol.* 506 860-76

Carroll TJ, Riek S and Carson RG 2001 Reliability of the input-output properties of the cortico-spinal pathway obtained from transcranial magnetic and electrical stimulation *J. Neurosci. Methods* 112 193-202

Castagnola E, Ansaldo A, Maggiolini E, Angotzi GN, Skrap M, Ricci D and Fadiga L 2013 Biologically compatible neural interface to safely couple nanocoated electrodes to the surface of the brain *ACS Nano* 7 3887–95

Castagnola E, Ansaldo A, Maggiolini E, Ius T, Skrap M, Ricci D and Fadiga L 2014 Smaller, softer,

lower-impedance electrodes for human neuroprosthesis: a pragmatic approach *Front. Neuroeng.* 7 8

Chiba A, Nakanishi H, Hiruma S, Satou T, Hashimoto S and Chichibu S 1992 Topographic mapping of the human motor cortex with magnetic stimulation: factors affecting accuracy and reproducibility *Electroencephalogr. Clin. Neurophysiol.* 85 9-16

Fernández E, Greger B, House PA, Aranda I, Botella C, Albisua J, Soto-sánchez C, Alfaro A and Normann RA 2014 Acute human brain responses to intracortical microelectrode arrays: challenges and future prospects *Front. Neuroeng.* 7 1–6

Hudson H, Griffin D and Belhaj-Saïf A 2010 Methods for chronic recording of EMG activity from large numbers of hindlimb muscles in awake rhesus macaques *J. Neurosci. Methods* 189 153-61

Huffman KJ and Krubitzer L 2001 Area 3a: topographic organization and cortical connections in marmoset monkeys *Cereb. Cortex* 11 849–67

Kleim JA, Barbay S and Nudo RJ 1998 Functional reorganization of the rat motor cortex following motor skill learning *J. Neurophysiol.* 80 3321–25

Kondo T, Yoshihara Y, Yoshino-Saito K, Sekiguchi T, Kosugi A, Miyazaki Y, Nishimura Y, Okano HJ, Nakamura M, Okano H, Isa T and Ushiba J 2015 Histological and electrophysiological analysis of the corticospinal pathway to forelimb motoneurons in common marmosets *Neurosci. Res.* 98 35-44

Landis JR and Koch GG 1977 The measurement of observer agreement for categorical data *Biometrics.* 33 159–74

Ludwig KA, Uram JD, Yang J, Martin DC and Kipke DR 2006 Chronic neural recordings using silicon microelectrode arrays electrochemically deposited with a poly(3,4-ethylenedioxythiophene) (PEDOT) film *J. Neural Eng.* 3 59-70

Lui LL, Mokri Y, Reser DH, Rosa M and Rajan R 2014 Responses of neurons in the marmoset primary auditory cortex to interaural level differences: comparison of pure tones and vocalizations *Front. Neurosci.* 9 132

MacDougall M, Nummela SU, Coop S, Disney A, Mitchell JF and Miller CT Optogenetic manipulation of neural circuits in awake marmosets *J. Neurophysiol.* 116 1286-94

Malcolm MP, Triggs WJ, Light KE, Shechtman O, Khandekar G and Gonzalez Rothi LJ 2006 Reliability of motor cortex transcranial magnetic stimulation in four muscle representations *Clin. Neurophysiol.* 117 1037-46

McGraw KO and Wong SP 1996. Forming inferences about some intraclass correlation coefficients *Psychol. Methods* 1 30–46

Mishory A, Molnar C, Kozel FA and George MS 2004 The maximum-likelihood strategy for determining transcranial magnetic stimulation motor threshold, using parameter estimation by sequential testing is faster than conventional methods with similar precision *J. ECT* 20 160-5

Molina-Luna K, Buitrago MM, Hertler B, Schubring M, Haiss F, Nisch W, Schulz JB and Luft AR 2007 Cortical stimulation mapping using epidurally implanted thin-film microelectrode arrays *J. Neurosci. Methods* 161 118–25

Molina-Luna K, Hertler B, Buitrago M and Luft AR 2008 Motor learning transiently changes cortical somatotopy *NeuroImage* 40 1748–54

Monfils M, Plautz EJ and Kleim JA 2005 In Search of the Motor Engram: Motor Map Plasticity as a Mechanism for Encoding Motor Experience *Neuroscientist* 11 471–83

Ngomo S, Leonard G, Moffet H and Mercier C 2012 Comparison of transcranial magnetic stimulation measures obtained at rest and under active conditions and their reliability *J. Neurosci. Methods* 205 65-71

Nudo RJ, Milliken GW, Jenkins WM and Merzenich MM 1996 Use-Dependent Primary Motor Alterations of Movement Representations Cortex of Adult Squirrel Monkeys *J. Neurosci.* 16 785–807

Nudo RJ and Milliken GW 1996 Reorganization of movement representations in primary motor cortex following focal ischemic infarcts in adult squirrel monkeys *J. Neurophysiol.* 75 2144–49

Okano H, Hikishima K, Iriki A and Sasaki E 2012 The common marmoset as a novel animal model system for biomedical and neuroscience research applications *Semin. Fetal. Neonatal. Med.* 17 336–40

Park MC, Belhaj-Saïf A and Cheney PD 2000 Chronic recording of EMG activity from large numbers of forelimb muscles in awake macaque monkeys *J. Neurosci. Methods* 96 153–60

Pentland A 1980 Maximum likelihood estimation: the best PEST *Percept. Psychophys.* 28 377–9

Qi F, Wu AD and Schweighofer N 2011 Fast estimation of transcranial magnetic stimulation motor threshold *Brain Stimul.* 4 50-7

Raineteau O and Schwab ME 2001 Plasticity of motor systems after incomplete spinal cord injury *Nat. Rev. Neurosci.* 2 263-73

Rossini PM, Barker AT, Berardelli A, Caramia MD, Caruso G, Cracco RQ, Dimitrijević MR, Hallett M, Katayama Y and Lücking CH 1994 Non-invasive electrical and magnetic stimulation of the brain, spinal cord and roots: basic principles and procedures for routine clinical application. Report of an IFCN committee *Electroencephalogr. Clin. Neurophysiol.* 91 79-92

Rousche PJ and Normann RA 1998 Chronic recording capability of the Utah intracortical electrode array in cat sensory cortex *J. Neurosci. Methods* 82 1–15

Sadakane O, Masamizu Y, Watakabe A, Terada S, Ohtsuka M, Takaji M, Mizukami H, Ozawa K, Kawasaki H, Matsuzaki M and Yamamori T 2015 Long-Term Two-Photon Calcium Imaging of Neuronal Populations with Subcellular Resolution in Adult Non-human Primates *CellReports* 13 1989–99

Schieber MH 2001 Constraints on somatotopic organization in the primary motor cortex *J. Neurophysiol.* 86 2125–43

Shrout PE and Fleiss JL 1979 Intraclass correlations: uses in assessing rater reliability *Psychol. Bull.* 86 420-8

Slutzky MW, Jordan LR, Krieg T, Chen M, Mogul DJ and Miller LE 2010 Optimal spacing of

surface electrode arrays for brain-machine interface applications *J. Neural Eng*. 7 26004

Takemi M, Castagnola E, Ansaldo A, Ricci D, Fadiga L, Taoka M, Iriki A and Ushiba J 2017 Rapid Identification of Cortical Motor Areas in Rodents by High-Frequency Automatic Cortical Stimulation and Novel Motor Threshold Algorithm *Front. Neurosci*. 11 580

Takemi M, Kondo T, Yoshino-Saito K, Sekiguchi T, Kosugi A, Kasuga S, Okano HJ, Okano H and Ushiba J 2014 Three-dimensional motion analysis of arm-reaching movements in healthy and hemispinalized common marmosets *Behav. Brain Res.* 275 259-68

Tia B, Takemi M, Kosugi A, Castagnola E, Ansaldo A, Nakamura T, Ricci D, Ushiba J, Fadiga L and Iriki A 2017 Cortical control of object-specific grasp relies on adjustments of both activity and effective connectivity: a common marmoset study *J. Physiol.* 595 7203-21

van de Ruit M, Perenboom MJ and Grey MJ 2015 TMS brain mapping in less than two minutes *Brain Stimul.* 8 231-9

Wolf SL, Butler AJ, Campana GI, Parris TA, Struys DM, Weinstein SR and Weiss P 2004 Intra-subject reliability of parameters contributing to maps generated by transcranial magnetic stimulation in able-bodied adults *Clin. Neurophysiol.* 115 1740-47

Wongsarnpigoon A and Grill WM 2012 Computer-based model of epidural motor cortex stimulation: effects of electrode position and geometry on activation of cortical neurons *Clin. Neurophysiol.* 123 160-72

Zandieh S, Hopf R, Redl H, and Schlag MG 2003 The effect of ketamine/xylazine anesthesia on sensory and motor evoked potentials in the rat *Spinal Cord* 41 16-22